Journal of Low Temperature Physics (2020) 199:1137–1147
https://doi.org/10.1007/s10909-020-02366-w

Deployment of POLARBEAR-2A

Daisuke Kaneko[1] · S. Adachi[2] · P. A. R. Ade[3] · M. Aguilar Faúndez[4] · Y. Akiba[5,6] · K. Arnold[7] · C. Baccigalupi[9,10] · D. Barron[11] · D. Beck[12] · S. Beckman[8] · F. Bianchini[13] · D. Boettger[7] · J. Borrill[14,15] · J. Carron[16] · S. Chapman[17] · K. Cheung[8] · Y. Chinone[1,18] · K. Crowley[8] · A. Cukierman[19] · M. Dobbs[20] · R. Dűnner[21] · H. El-Bouhargani[12] · T. Elleflot[7] · J. Errard[12] · G. Fabbian[16] · S. M. Feeney[22] · C. Feng[23] · T. Fujino[24] · N. Galitzki[7] · A. Gilbert[20] · N. Goeckner-Wald[19] · J. Groh[8] · G. Hall[25] · N. W. Halverson[26,27] · T. Hamada[6,28] · M. Hasegawa[5,6] · M. Hazumi[1,5,6,29] · C. A. Hill[8,30] · L. Howe[7] · Y. Inoue[31] · G. Jaehnig[26,27] · O. Jeong[8] · N. Katayama[1] · B. Keating[7] · R. Keskitalo[14,15] · S. Kikuchi[24] · T. Kisner[14,15] · N. Krachmalnicoff[9] · A. Kusaka[1,30,32] · A. T. Lee[8,30,33] · D. Leon[7] · E. Linder[15,30] · L. N. Lowry[7] · A. Mangu[8,30] · F. Matsuda[1] · Y. Minami[5] · M. Navaroli[7] · H. Nishino[18] · J. Peloton[17] · A. T. P. Pham[13] · D. Poletti[9] · G. Puglisi[34] · C. L. Reichardt[13] · C. Ross[17] · Y. Segawa[5,6] · M. Silva-Feaver[7] · P. Siritanasak[7] · N. Stebor[36] · R. Stompor[12] · A. Suzuki[30] · O. Tajima[2] · S. Takakura[1] · S. Takatori[5,6] · D. Tanabe[5,6] · G. P. Teply[7] · T. Tomaru[35] · C. Tsai[7] · C. Verges[12] · B. Westbrook[30] · Y. Zhou[8]

Received: 20 September 2019 / Accepted: 27 January 2020 / Published online: 12 March 2020

Abstract
POLARBEAR-2A is the first of three receivers in the Simons array, a cosmic microwave background experiment located on the Atacama Plateau in Chile. POLARBEAR-2A was deployed and achieved the first light in January 2019 by mapping the microwave emission from planet observations. Commissioning work is underway to prepare the receiver for science observations.

Keywords CMB · *B*-mode polarization · Millimeter wave · TES bolometer

✉ Daisuke Kaneko
daisuke.kaneko@ipmu.jp

Extended author information available on the last page of the article

1 Introduction

1.1 Motivations for B-Mode Studies

Since its discovery in 1964, the cosmic microwave background (CMB) has been one of the most important sources of cosmological information. Many observations have been performed since then, and observation technology has also greatly advanced (see review in [1] and references therein). A front line is the observation of B-mode polarization, which is a pattern characterized by odd-parity in spatial inversion.

The goal of B-mode polarization observation is to provide evidence of a nonzero tensor-to-scalar ratio, r. It is defined as the ratio of the amplitudes of the tensor and scalar perturbations in the early universe. Tensor perturbations are only caused by primordial gravitational waves that are generated by cosmic inflation [2, 3]. Therefore, a nonzero r would provide evidence of the inflation, and if discovered, the value of r would help to distinguish between inflation models. Another motivation for observing B-mode is to measure the sum of neutrino masses $\Sigma_{i=1}^{3} m_\nu^i$ [4, 5]. The B-mode anisotropies at small scales arise from E-mode by the effect of gravitational lensing, which are sensitive to $\Sigma_{i=1}^{3} m_\nu^i$.

1.2 Concept of POLARBEAR and Simons Array Experiments

The POLARBEAR (PB) experiment is designed to observe the CMB polarization and is mounted on the Huan Tran Telescope (HTT). With a primary mirror of 2.5 m effective diameter and with a continuously rotating half-wave plate (HWP) [6], PB achieved high sensitivity across a wide multipole range where both primordial gravitational waves and gravitational lensing B-modes are included. The original PB experiment began PB-1 observations in year 2012. Our results were published in papers [7–12].

The Simons Array (SA) is an upgrade of the PB experiment with three telescopes with newly designed receivers. Two additional telescopes of the same design[1] have been built next to the original HTT. The new receivers are called POLARBEAR-2A (PB-2A), POLARBEAR-2B (PB-2B), and POLARBEAR-2C (PB-2C), respectively, by the order in which they are manufactured. The number of detectors per receiver is 7588: about six times more than that of PB-1. PB-2A and PB-2B are equipped with dichroic sensors to detect 90 GHz and 150 GHz bands. PB-2C also has dichroic sensors, but these are sensitive to frequency bands centered at 220 and 270 GHz to detect thermal dust radiation. Because of additional frequency bands, SA will be able to more reliably separate the CMB signal from those produced by foreground sources.

The expected sensitivities at SA are $\sigma(r) = 0.006$ for $r = 0.1$, and $\sigma(\Sigma_{i=1}^{3} m_\nu^i) = 40\,\mathrm{meV}$ for the sum of neutrino masses. Both values are in 68% C.L.,

[1] The Nicholas Simons Telescope (North) and The Paul Simons Telescope (South).

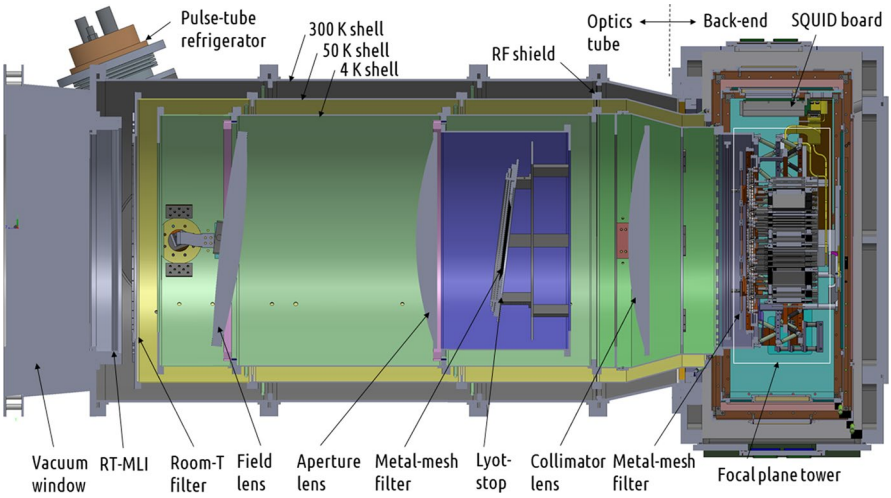

Fig. 1 Cross-sectional image of POLARBEAR-2A receiver. The cryostat has 300 K, 50 K, and 4 K shells. Light enters the receiver from foamed polypropylene window (50 cm diameter, 20 cm thickness) at the left side (Color figure online)

after 3 years of observation with expected performance, foreground reduced, and degeneracy mitigated with future optical surveys such as DESI [13].

2 Design of POLARBEAR-2A

A cross-sectional image of the PB-2A receiver is described in Fig. 1. The receiver can be separated into two sections: an "optics tube" and a "backend." CMB light enters the receiver through the window of the optics tube and finally focuses on the detector located at the backend.

2.1 Optical System

The HTT adopts a Gregorian–Dragone configuration [14] which can compensate for cross polarization made by each mirror. A receiver system is located around the Gregorian focus of the telescope. The POLARBEAR-2A receiver comprises a cryostat with three shells cooled by pulse tube refrigerators. The chambers inside are supported by insulating fiberglass laminate struts, and multilayer reflective insulators are installed to reduce thermal conduction. The outermost 300 K shell is also a vacuum chamber.

The optics tube contains a re-focusing optical system that consists of three alumina lenses. Details of fundamental optical design are found elsewhere [15]. To reduce reflections caused by the high refractive index (3.10) of alumina, two types of anti-reflection coatings are applied. A two-layered epoxy resin [16] is used for each curved face, and a sprayed mullite and porous-polyimide sheet [17] is used for each flat face. Radio transparent multi-layered insulators (RT-MLIs [18]), an

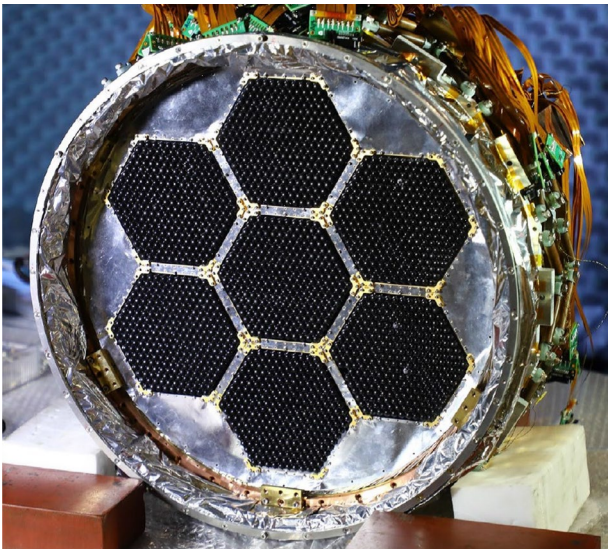

Fig. 2 Assembled focal plane tower. Each with the seven hexagonal structure is a detector module, and the surface is covered with lenslets (Color figure online)

alumina filter and low-pass metal mesh filters are installed in the optical system to reduce the thermal load. The aperture (Lyot) stop is put inside the 4 K shell, and tile-shaped epoxy-based black body (KEK-black) [19] is mounted at its surface. The same black-body absorber is applied to the inner surface of the 4 K shell.

2.2 Detector

Figure 2 shows the PB-2A detectors assembled in the focal plane tower (FPT). A 3-stage He sorption refrigerator cools the FPT. Seven detector modules are attached to the stage of 0.3 K. Each detector module comprises a detector wafer inserted in an Invar wafer holder, lenslets, and readout modules for multiplexing readout. PB-2A adopts transition edge sensor (TES) bolometer technology [20, 21]. The TES utilizes a very steep resistance change at superconducting transition. The TES of PB-2A is composed of an AlMn alloy and is operated with constant voltage bias.

The incident photons are coupled to an antenna by a silicon lenslet. Figure 3 provides a zoomed-in photograph of a sinuous antenna. It is sensitive to two orthogonal linear polarizations and provides uniform response over a wide frequency range. A load resistor coupled with the antenna and the TES are on an "island," and heat from the load resister transmits to the TES.

2.3 Readout System

A schematic of the TES readout is shown in Fig. 4 [22]. PB-2A uses Digital Frequency-Division Multiplexing (DfMux) of factor 40 to reduce the thermal loading

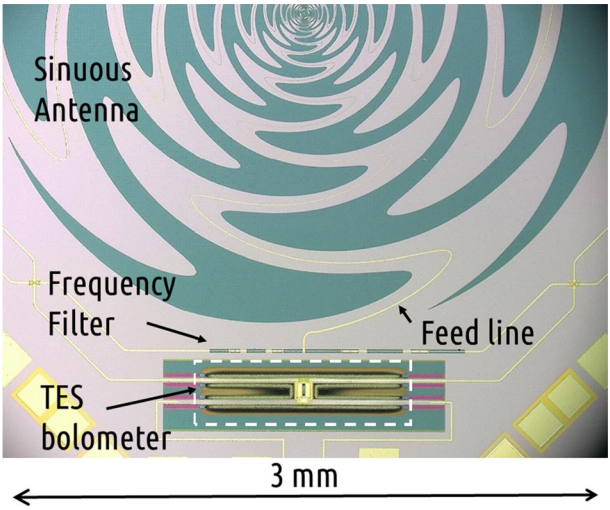

Fig. 3 Microscopic image of sinuous antenna and detector which are processed on a silicon wafer. The TES is located at the center of dashed rectangle (Color figure online)

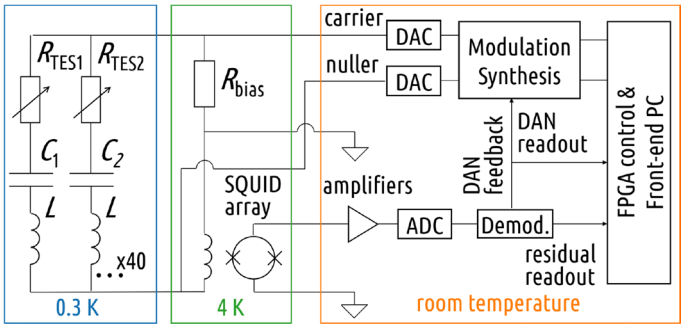

Fig. 4 Schematic diagram of PB-2A readout. Stages of different temperatures are thermally insulated with NbTi cable (0.3–4 K) and flexible wire harness (4 K—room Temp.) (Color figure online)

from outer electronics, and the total number of cables. In the DfMux method, TESs are coupled with LC resonators of different resonant frequencies and bias voltages are supplied in corresponding mixed frequencies. The multiplexed TES currents travel over low-inductance thermally insulating cables where they are transduced into a voltage by a SQUID array operating at 4 K. Input signal generation, output digitization, and network communication are controlled with "ICE boards" [23], FPGA-based electronics, installed in telescope comoving crates. The sampling frequency is 152 Hz for all channels. Data stored at the front-end computer is transferred down-site to the foot of the mountain by a direct radio-link, subsequently, transferred to servers located in the USA and Japan using the Internet.

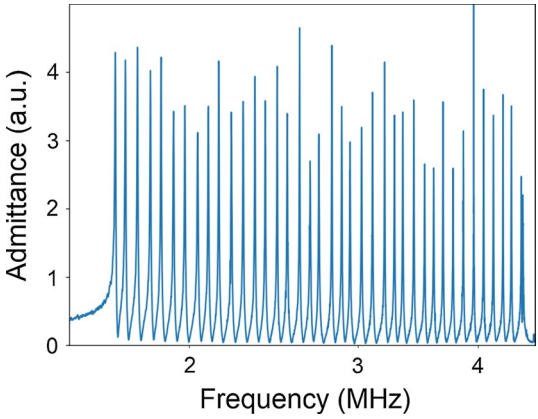

Fig. 5 40 Different LC resonant peaks seen in laboratory test (Color figure online)

3 Validation of POLARBEAR-2A

3.1 Laboratory Testing

Integration tests of the PB-2A receiver were conducted with a fully installed detector array and nearly all readout channels until the summer of 2018 at KEK, Japan. There are several fundamental functionalities that had to be confirmed before shipping to the site: (a) evacuation and cooling with refrigerators, (b) data acquisition tests with equivalent setup as the site, and (c) optical performance at cryogenic temperature.

The evacuation and cooling were tested successfully at nominal operation temperature at 0.3 K for the detector stage. The typical hold time was 20 h, which is long enough to operate in a 24-h cycle. As this value is under a condition with additional neutral density filters for laboratory tests, the hold time should be a few hours longer without the filters at the site. Second, data acquisition was checked with full-scale TES channels under the same hardware configuration as that at the site [24]. Figure 5 shows an example of the DfMux readout, in which 40 peaks corresponding to multiplexed channels are clearly seen. The receiver noise was checked to ensure that the dominant noise was photon noise but not readout noise ($\sim 20\,\mathrm{pA}/\sqrt{\mathrm{Hz}}$ in normal conduction state). Third, the optical transmission of optics tube was confirmed. The optical efficiency from the window to the detector was measured with a liquid nitrogen vessel placed in front of the window. The optical efficiency was found to be 23%/21% for 90/150 GHz band, which is consistent with the expectation.

The spectral performance of the detector was examined with a Fourier-transform spectrometer [25]. Some TESs of both bands are measured. Measured band centers were 85.2/143.9 GHz and band widths were 18.3/22.1 GHz for 90/150 GHz band channels, which were within the expected ranges. Spectroscopic tests for the entire detector array are planned at the site. The detectors were upgraded after these measurements. Detection efficiency is expected to be improved with upgraded detectors that use silicon nitride as the dielectric [21]. Operation of calibrators like a stimulator (described later) is also tested in the laboratory.

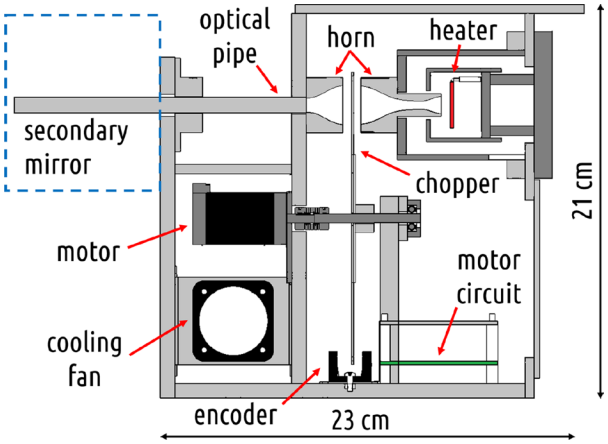

Fig. 6 Design of the stimulator for PB-2A. A ceramic heater (700 °C) is covered in total three layers of covers. The chopper modulates signal from 5 to 44 Hz (Color figure online)

3.2 Site Commissioning

In October 2018, the receiver was shipped to the Atacama Plateau. The assembly and installation onto the north telescope were completed in about one month and subsequently, site commissioning began. The cryogenic system was soon stabilized to enable test operation, then readout tests were successively performed. The achieved noise in the best case at the site is $\sim 15\,\mathrm{pA}/\sqrt{\mathrm{Hz}}$ (in normal conduction state). The assembly and operation test of the HWP have been finished.

3.2.1 Stimulator

The stimulator is an artificial calibration source that uses black-body radiation from a ceramic heater (see Fig. 6). It is placed behind the secondary mirror, and signal is sent through a small hole in the mirror. In normal observations, stimulator data will be taken before and after each CMB scan and used for channel selection, relative gain calibration, and time-constant measurements. It is also used for many tests in deployment as a constant source. The signal was clearly seen with sufficient intensity by most ($> 90\%$) of the available detectors. Measured effective temperature is 45/70 mK for 90/150 GHz bands.

3.2.2 Planet Observations

Planet observations are useful for beam-shape characterization because planets are effectively point-like sources. We achieved the first light with an observation of Venus in January 2019. Figure 7 is the first planet image which we observed with POLARBEAR-2A. Although the telescope had not yet been optimally aligned at this stage, data from several detectors during this scan showed circular images of Venus.

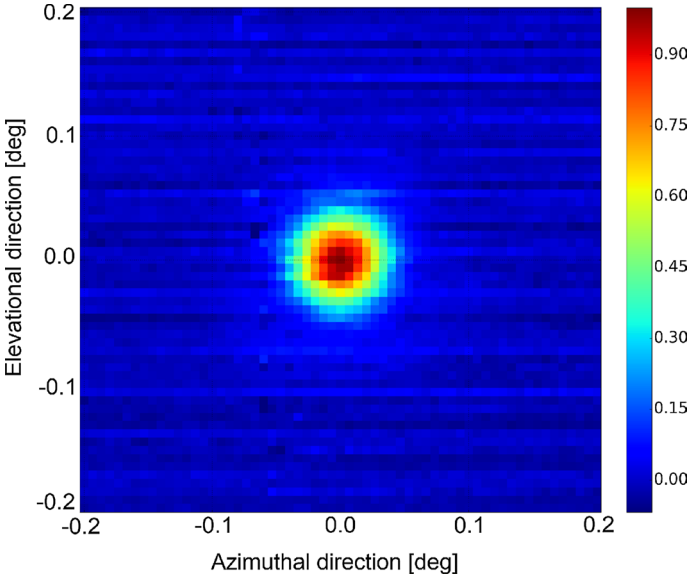

Fig. 7 Observed image of Venus averaged over 150 GHz TESs in one detector module. This is a preliminary image before alignment of the receiver (Color figure online)

Measured beam widths were 5.8/3.8 arcmin in FWHM for 90/150 GHz channels, while design values are 5.2/3.5 arcmin. More recently, other planets such as Jupiter and Saturn have been observed as well. These planet images are being used for alignment of the telescope and absolute scale calibration.

4 Conclusion

PB-2A, the first receiver for the Simons Array, is expected to have higher performance than the original PB-1, with about 6 times as many TES detectors as those of PB-1. Laboratory tests were finished, and the PB-2A was deployed to the site in the Atacama Plateau. We achieved a successful operation of thousands of TESs, and the first light with PB-2A was received in planet observations. The commissioning work continues to validate all the systems to start CMB science observations.

Acknowledgements The Simons Array is supported by the Simons Foundation, the National Science Foundation grant (AST-0618398, AST-1212230, AST-1440338), NASA grant NNG06GJ08G, the Moore Foundation (GBMF4633), the Heising-Simons Foundation, Templeton Foundation grant number 58724, the Ax Center for Experimental Cosmology at UC San Diego, the U.S. Department of Energy, Office of Science, Office of High Energy Physics, JSPS KAKENHI Grant Number (JP26220709, JP15H03670, JP15H05891, JP18H01240), and JSPS Core-to-core Program, A. Advanced Research Networks.

Kavli IPMU authors are supported by World Premier International Research Center Initiative (WPI), MEXT, Japan.

The McGill authors acknowledge the Natural Sciences and Engineering Research Council and Canadian Institute for Advanced Research, National Commission for Scientific and Technological Research. The SISSA authors acknowledge support from the ASI-COSMOS network (cosmosnet.it) and the INDARK INFN Initiative.

The James Ax Observatory operates in the Parque Astronomico Atacama in Northern Chile under the auspices of the Comision Nacional de Investigacion Cientifica y Tecnologica de Chile (CONICYT).

References

1. R. Durrel, Class. Quantum Gravity **32**, 12 (2015). https://doi.org/10.1088/0264-9381/32/12/124007
2. U. Seljak, M. Zaldarriaga, Phys. Rev. Lett. **78**, 2054 (1997)
3. M. Kamionkowski, A. Kosowsky, A. Stebbins, Phys. Rev. Lett. **78**, 2058 (1997)
4. D.J. Eisenstein, W. Hu, M. Tegmark, Astrophys. J. **518**(2), 23 (1998)
5. M. Kaplinghat, L. Knox, Y.-S. Song, Phys. Rev. Lett. **91**, 241301 (2003)
6. C.A. Hill et al., Proc. SPIE (2016). https://doi.org/10.1117/12.2232280
7. P.A.R. Ade et al. (POLARBEAR Collaboration), Phys. Rev. Lett. **112**, 131302 (2014)
8. P.A.R. Ade et al. (POLARBEAR Collaboration), Astrophys. J. **794**(2), 171 (2014)
9. P.A.R. Ade et al. (POLARBEAR Collaboration), Phys. Rev. Lett. **113**, 021301 (2014)
10. J. Errard et al. (POLARBEAR Collaboration), Astrophys. J. **809**, 63 (2015)
11. P.A.R. Ade et al. (POLARBEAR Collaboration), Phys. Rev. D **92**, 123509 (2015)
12. P.A.R. Ade et al. (POLARBEAR Collaboration), Astrophys. J. **848**, 121 (2017)
13. A. Aghamousa, et al. (The DESI Collaboration). arXiv:1611.00036 [astro-ph.IM] (2016)
14. C. Dragone, Bell Syst. Tech. J. **57**, 7 (1978)
15. F.T. Matsuda, Doctoral Thesis, University of California San Diego (2017)
16. D. Rosen et al., Appl. Opt. **52**, 33 (2013). https://doi.org/10.1364/AO.52.008102
17. Y. Inoue et al., Appl. Opt. **55**, 34 (2016). https://doi.org/10.1364/AO.55.000D22
18. J. Choi et al., Rev. Sci. Instrum. **84**, 114502 (2013). https://doi.org/10.1063/1.4827081
19. Y. Inoue, Doctoral Thesis, Graduate University for Advanced Studies (SOKENDAI) (2016)
20. K.D. Irwin, G.C. Hilton, Cryogenic Particle Detection, in *Cryogenic Particle Detection*, ed. by C. Enss (Springer, Berlin, 2005)
21. B. Westbrook et al., J. Low Temp. Phys. **193**, 758 (2018). https://doi.org/10.1007/s10909-018-2059-0
22. K. Hattori et al., Nucl. Instrum. Methods A **732**, 299–302 (2013). https://doi.org/10.1016/j.nima.2013.07.052
23. K. Bandura et al., J. Astron. Instrum. **05**, 1641005 (2017)
24. D. Barron et al., Proc. SPIE (2018). https://doi.org/10.1117/12.2311502
25. F. Matsuda et al., Rev. Sci. Instrum. **90**, 115115 (2019). https://doi.org/10.1063/1.5095160. arXiv:1904.02901 [astro-ph.IM]

Affiliations

Daisuke Kaneko[1] · S. Adachi[2] · P. A. R. Ade[3] · M. Aguilar Faúndez[4] · Y. Akiba[5,6] · K. Arnold[7] · C. Baccigalupi[9,10] · D. Barron[11] · D. Beck[12] · S. Beckman[8] · F. Bianchini[13] · D. Boettger[7] · J. Borrill[14,15] · J. Carron[16] · S. Chapman[17] · K. Cheung[8] · Y. Chinone[1,18] · K. Crowley[8] · A. Cukierman[19] · M. Dobbs[20] · R. Dűnner[21] · H. El-Bouhargani[12] · T. Elleflot[7] · J. Errard[12] · G. Fabbian[16] · S. M. Feeney[22] · C. Feng[23] · T. Fujino[24] · N. Galitzki[7] · A. Gilbert[20] · N. Goeckner-Wald[19] · J. Groh[8] · G. Hall[25] · N. W. Halverson[26,27] · T. Hamada[6,28] · M. Hasegawa[5,6] · M. Hazumi[1,5,6,29] · C. A. Hill[8,30] · L. Howe[7] · Y. Inoue[31] · G. Jaehnig[26,27] · O. Jeong[8] · N. Katayama[1] · B. Keating[7] · R. Keskitalo[14,15] · S. Kikuchi[24] · T. Kisner[14,15] · N. Krachmalnicoff[9] · A. Kusaka[1,30,32] · A. T. Lee[8,30,33] · D. Leon[7] · E. Linder[15,30] · L. N. Lowry[7] · A. Mangu[8,30] · F. Matsuda[1] · Y. Minami[5] · M. Navaroli[7] · H. Nishino[18] · J. Peloton[17] · A. T. P. Pham[13] · D. Poletti[9] · G. Puglisi[34] · C. L. Reichardt[13] · C. Ross[17] · Y. Segawa[5,6] · M. Silva-Feaver[7] · P. Siritanasak[7] · N. Stebor[36] · R. Stompor[12] · A. Suzuki[30] · O. Tajima[2] · S. Takakura[1] · S. Takatori[5,6] · D. Tanabe[5,6] · G. P. Teply[7] · T. Tomaru[35] · C. Tsai[7] · C. Verges[12] · B. Westbrook[30] · Y. Zhou[8]

[1] Kavli Institute for the Physics and Mathematics of the Universe (WPI), UTIAS, The University of Tokyo, Kashiwa, Chiba 277-8583, Japan

[2] Department of Physics, Kyoto University, Kyoto, Japan

[3] School of Physics and Astronomy, Cardiff University, Cardiff, UK

[4] Departamento de Física, FCFM, Universidad de Chile, Santiago, Chile

[5] High Energy Accelerator Research Organization (KEK), Ibaraki, Japan

[6] The Graduate University for Advanced Studies (SOKENDAI), Ibaraki, Japan

[7] Department of Physics, University of California, San Diego, USA

[8] Department of Physics, University of California, Berkeley, USA

[9] The International School for Advanced Studies (SISSA), Trieste, Italy

[10] The National Institute for Nuclear Physics (INFN), Trieste, Italy

[11] Department of Physics and Astronomy, University of New Mexico, Albuquerque, USA

[12] AstroParticule et Cosmologie, Université Paris Diderot, Paris, France

[13] School of Physics, University of Melbourne, Melbourne, Australia

[14] Space Sciences Laboratory, University of California, Berkeley, USA

[15] Computational Cosmology Center, Lawrence Berkeley National Laboratory, Berkeley, USA

[16] Department of Physics and Astronomy, University of Sussex, Brighton, England

[17] Department of Physics and Atmospheric Science, Dalhousie University, Halifax, Canada

[18] Research Center for the Early Universe, School of Science, The University of Tokyo, Tokyo, Japan

[19] Kavli Institute for Particle Astrophysics and Cosmology, Stanford University, Stanford, USA

[20] Department of Physics, McGill University, Montreal, Canada

[21] Instituto de Astrofísica and Centro de Astro-Ingeniería, Facultad de Física, Pontificia Universidad Católica de Chile, Santiago, Chile

[22] Center for Computational Astrophysics, Flatiron Institute, New York, USA

[23] Department of Physics, University of Illinois at Urbana-Champaign, Champaign, USA

[24] Graduate School of Engineering Science, Yokohama National University, Kanagawa, Japan

[25] School of Physics and Astronomy, University of Minnesota, Minneapolis, USA

[26] Center for Astrophysics and Space Astronomy, Department of Astrophysical and Planetary Sciences, University of Colorado, Boulder, USA

[27] Department of Physics, University of Colorado, Boulder, USA

[28] Astronomical Institute, Graduate School of Science, Tohoku University, Miyagi, Japan

[29] Institute of Space and Astronautical Science (ISAS), Japan Aerospace Exploration Agency (JAXA), Kanagawa, Japan

[30] Physics Division, Lawrence Berkeley National Laboratory, Berkeley, USA

[31] Department of Physics, National Central University, Zhongli, Taiwan

[32] Department of Physics, School of Science, The University of Tokyo, Tokyo, Japan

[33] Radio Astronomy Laboratory, University of California, Berkeley, USA

[34] Department of Physics, Stanford University, Stanford, USA

[35] National Astronomical Observatory of Japan (NAOJ), Tokyo, Japan

[36] Intel Corporation, Santa Clara, USA